The aerodynamics of revolving wings

II. Propeller force coefficients from mayfly to quail

James R. Usherwood* and Charles P. Ellington

Department of Zoology, University of Cambridge, Downing Street, Cambridge CB2 3EJ, UK

*Present address: Concord Field Station, MCZ, Harvard University, Old Causeway Road, Bedford, MA 01730, USA
(e-mail: jimusherwood@lycos.co.uk)

Summary

High force coefficients, similar to those observed for revolving model hawkmoth wings in the accompanying paper (for which steady leading-edge vortices are directly observed), are apparent for revolving model (mayfly, bumblebee and quail) and real (quail) animal wings ranging in Reynolds number (Re) from 1100 to 26 000. Results for bumblebee and hawkmoth wings agree with those published previously for *Drosophila* ($Re \approx 200$). The effect of aspect ratio is also tested with planforms based on hawkmoth wings adjusted to aspect ratios ranging from 4.53 to 15.84 and is shown to be relatively minor, especially at angles of incidence below 50°.

The normal force relationship introduced in the accompanying paper is supported for wings over a large range of aspect ratios in both 'early' and 'steady' conditions; local induced velocities appear not to affect the relationship.

Key words: aerodynamics, flight, propeller, force coefficient, lift, drag, wing.

Introduction

High force coefficients are required to account for hovering flight in animals ranging from small insects (e.g. Ellington, 1984a–f) to medium-sized birds (Norberg, 1975) and bats (Norberg, 1976). Ellington et al. (1996) showed leading-edge vortices to be present over flapping real and model hawkmoth wings. These leading-edge vortices, created by dynamic stall and maintained by spanwise flow, contribute significantly to lift production in slow-flying hawkmoths. The accompanying paper (Usherwood and Ellington, 2002) shows this phenomenon, and high force coefficients, to be a stable aerodynamic characteristic of revolving model moth wings. The present paper aims to determine how robust this characteristic is to variations in wing design and Reynolds number. Model hawkmoth wings with a range of aspect ratio and real and model wings from a number of 'key species' are tested.

Aspect ratio

The basic planform shape of many animal wings may be characterized in simple terms (Weis-Fogh, 1973; Ellington, 1984b). One key variable is the aspect ratio $A\!R$ of the wing:

$$A\!R = 4R^2/S, \tag{1}$$

where S is the total wing area and R is the single wing length. Most flying animals are functionally two-winged; many four-winged insects link fore- and hindwings, and, for these morphological parameters, the linked wings are treated as one. Standard hawkmoth planforms (Usherwood and Ellington, 2002), with their chords scaled by ×0.4, ×0.6, ×0.8, ×1 and ×1.4, are tested in this study, resulting in five wing designs with constant wing length and an aspect ratio range of 4.53–15.84. Scaling the chord produces reasonably insect-wing-like planforms with the variation of a single parameter.

Insects have wings of $A\!R$ ranging from 2.8 (butterflies, Dudley and DeVries, 1990) to 10.9 (craneflies, Ellington, 1984b). Vertebrates capable of hovering have wings ranging in $A\!R$ from 4.4 (pied flycatcher, Norberg, 1975) to 8.2 (hummingbirds, Wells, 1993). The aspect ratios of the wings in this study range from 4.53 to 15.84, and angles of incidence greater than 90° are tested, so our results are relevant to studies of animals that hover using a vertical stroke plane or swim using drag-based propulsion.

Conventional propellers and wind turbines revolve, but delayed stall and high force coefficients typically exist only at the wing (rotor) bases [Himmelskamp in Schlichting, 1968 (propellers); Graham, 1992 (wind turbines)]. Otherwise, flow over high-$A\!R$ propellers and turbines at high angles of incidence stalls conventionally, and blade-element analyses using coefficients derived from steady, two-dimensional flow conditions are effective. So, it is reasonable to expect that the high-lift mechanisms described by Usherwood and Ellington (2002) for wings of $A\!R$=6.34 might gradually or suddenly decline with increasing aspect ratio.

The implications of Reynolds number for flight

Reynolds number Re has a large impact on the behaviour of fluids flowing past an object; Vogel (1981) presents the concepts clearly in a biological context. It is therefore reasonable to expect Re to have a similar bearing on the flow (and so lift and drag) acting on wings. Indeed, it is frequently supposed that many of the unexpected phenomena associated with insect flight may be accounted for by the low values of Re at which they operate. However, predictions based on Re arguments are not always founded; while it is true that viscous drag forces are higher for smaller animals, it is not true that the very small and 'fringe-winged' insects ($Re<28$) 'row' through the air using drag-based mechanisms (Ellington, 1984a). Indeed, the vertical stroke plane associated with drag-based weight support is surprisingly seen in larger insects (butterflies) at Re values of approximately 2800 (Maxworthy, 1981; Ellington, 1984a; Sunada et al., 1993).

So, at this stage, it is unclear whether insects, small, and even large, vertebrates operate in the same flow regime; it is not known whether there are significant qualitative differences in flow analogous to the transition between laminar and turbulent conditions. Is there a subtle gradient from one regime to another (this does not appear likely given the properties of normal laminar/turbulent transitions)? Or is there a biologically significant threshold above (or below) which certain aerodynamic mechanisms are unable to operate? If so, where are these boundaries?

Key species

To gain more information of biological interest, this study investigates several key species for which the appropriate parameters are known. Bees are of particular interest as they show a considerable size range both within a species (between different castes of bumblebee) and among related genera (e.g. the Euglossini or orchid bees). A bumblebee wing was therefore tested to provide information on the aerodynamic properties of wings in revolution for an insect for which there is a great deal of morphological, kinematic and energetic data (Dudley and Ellington, 1990a,b; Cooper, 1993) and which should also be applicable to studies of euglossine bees (Casey and Ellington, 1989; Dudley, 1995; Dudley and Chai, 1996).

To determine the steady aerodynamic performance of wings in revolution at low and high Re, a 'mini-spinner' was built covering the range of Re from 1100 to 26 000. The model animals chosen for these extremes were the mayfly *Ephemera vulgata* and blue-breasted quail *Coturnix chinensis*, for which fresh wings were available. The 'mini-spinner', a smaller and simplified version of the more elaborate propeller described in Usherwood and Ellington (2002), proved a robust and effective tool. It also allowed the use of real bird wings over a limited size range, so both real and model quail wings were tested.

Inferring the presence of a leading-edge vortex

Smoke observations for simple model hawkmoth wings by Usherwood and Ellington (2002) supported the finding (Ellington et al., 1996) that the mechanism for high lift is a leading-edge vortex. However, wing speeds and designs in the present study precluded such observations. As shown in Usherwood and Ellington (2002), flow separation can nevertheless be inferred if the resultant force is approximately normal to the wing surface.

Materials and methods

Force measurements were made using two experimental propellers. The larger design, described by Usherwood and Ellington (2002), allows 'early' (from the first half-revolution) and 'steady' vertical and horizontal forces to be measured using foil strain gauges. The smaller, much simpler, design could only measure 'steady' forces, but could do so over a much larger speed range.

Vertical and horizontal force coefficients were derived from measured vertical forces and torques as described by Usherwood and Ellington (2002). Following Usherwood and Ellington (2002), the term 'propeller coefficient' is used to distinguish force coefficients derived from propeller experiments.

Large propeller experiments

Unless otherwise stated, all aspects of the experimental method for the large propeller experiments were identical to those described by Usherwood and Ellington (2002). Methods of wing construction, force measurement and data processing were suitable for a limited Re range, appropriate for hawkmoths and queen bumblebees.

Aspect ratio

The standard hawkmoth planform was adapted to produce wing pairs with a range of five aspect ratios (Fig. 1A): all wings were thin and flat. The wing length in every case, including the offset due to the method of attachment to the propeller head (see Usherwood and Ellington, 2002), was 556 mm, and the relevant second, $\hat{r}_2(S)$, and third, $\hat{r}_3(S)$, non-dimensional wing moments of area remained constant: $\hat{r}_2(S)=0.547$ and $\hat{r}_3(S)=0.588$. Wing thickness was constrained by the material used, and the angular velocity was kept constant. The mean wing thickness (relative to mean chord) and Re (defined using the conventions of Ellington, 1984f) were therefore confounding variables (Table 1). The constant angular velocity also resulted in smaller signal-to-noise ratios for higher-$A\!R$ (narrower) wings, because they experienced smaller forces.

Bumblebee

The planform for a bumblebee (Fig. 1B) *Bombus terrestris* wing design was taken from a previous study and used to produce a wing pair as described for the hawkmoth (Usherwood and Ellington, 2002). Bumblebee B27 was selected because its aspect ratio and radii for moments of area were the closest to the population means. Again, the wing shape was kept constant so that the offset due to the attachment of the wings to the propeller head changed the wing moments, as shown in Table 2.
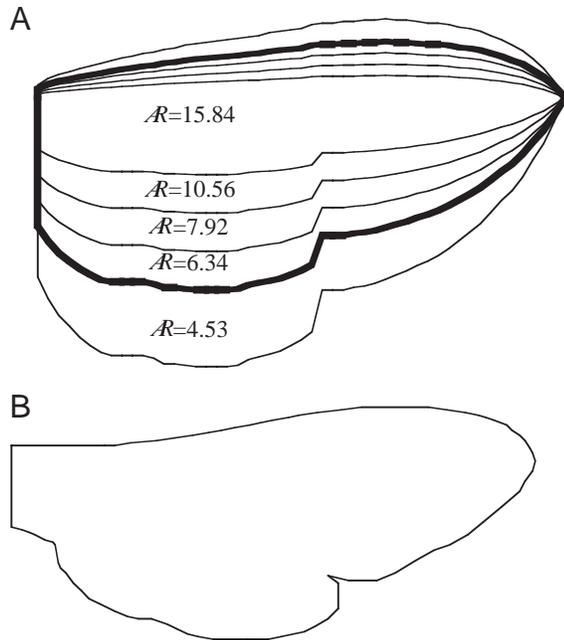
Fig. 1. Model hawkmoth planforms with a range of aspect ratios ($A\!R$) (A) and bumblebee planform (B). Wing lengths R: model hawkmoth R=0.5 m; real bumblebee R=12.86 mm; model bumblebee R=0.5 m.

Table 1. *Confounded variables with variation in aspect ratio*

Wing type (aspect ratio)	Wing thickness (% of wing chord)	Reynolds number
15.84 (very narrow)	3.91	3230
10.56	2.61	4846
7.92	1.96	6461
6.34 (standard)	1.57	8071
4.53 (wide)	1.12	11 295

random air movements; random air movements will be negligible compared with the flow generated by the wings. The size and relative stiffness of the mini-spinner also allows the use of real bird wings. The extremes in *Re* are represented by model mayfly forewings and both model and real quail wings.

Wing design

Model mayfly forewings were based on those from a 26.4 mg male mayfly *Ephemera vulgata* (Fig. 3A). The hindwings were not included in the model because they were small and their orientation during flapping flight was unknown. The planform was maintained, so the small shift due to the diameter of the rotor head (of diameter 9 mm, causing an offset of 4.5 mm) influences the wing moments. Table 2 shows the resulting wing parameters.

The model mayfly wings were constructed from stiff, thin (0.15 mm) card glued to 0.57 mm diameter wire running half-way down the ventral surface of the wing. This resulted in a wing thickness at the position of mean chord of 5 % of wing chord.

Geometric angles of attack were set by rotating the wire wing-stems within the propeller head and measured using a inclinometer, which achieved an estimated accuracy of ±2 °. Angles from 0 to 90 ° were used, with 10 ° increments. The angles of incidence were calculated as in Usherwood and Ellington (2002).

A 61.6 g blue-breasted quail *Coturnix chinensis* was killed by decapitation as part of another study (Askew et al., 2001). The right wing (fresh mass 2.29 g) was removed at the base of the humerus and pinned to dry using hypodermic needles. The pinned position mimicked a typical mid-downstroke position determined from the video recordings of ascending flight used by Askew et al. (2001). Once stiff, the wing was connected

The propeller was driven slightly more slowly than for the hawkmoth tests, at 0.147 Hz, thus reducing the Reynolds number to 5496, a value appropriate for the largest queen bumblebees and large euglossines. Further reduction in speed produced very noisy results because of dominating mechanical oscillations, while reducing the wing length would have confounded the effects of the offset, which otherwise was kept constant for experiments on the large propeller.

Small propeller ('mini-spinner') experiments

Fig. 2 shows the basic construction of the 'mini-spinner'. It uses the same principle for the measurement of vertical forces (moments about a knife-blade fulcrum, forming a 'see-saw') as used by Usherwood and Ellington (2002) but different principles for torques. Unsteady force measurements and flow visualisations are impossible with the mini-spinner, but the smaller size requires higher frequencies of revolution for *Re* similarity, with the advantage that low-*Re* models can be used while minimising the effects of

Table 2. *Morphological parameters for real and model wings*

	Bombus B27	Model bumblebee wing with offset	Real mayfly forewing	Real mayfly hindwing	Combined real mayfly wings	Model mayfly forewing	Quail wing	Real or model quail wing including offset
R (mm)	12.86	556	13.0	3.9	13.0	54.5	100.1	104.6
$A\!R$	6.32	7.13	6.42	5.10	5.77	7.67	4.52	4.93
$\hat{r}_2(S)$	0.541	0.578	0.546	0.572	0.520	0.573	0.522	0.538
$\hat{r}_3(S)$	0.585	0.614	0.588	0.610	0.568	0.609	0.567	0.580

R, wing length; $A\!R$, aspect ratio; $\hat{r}_2(S)$ and $\hat{r}_3(S)$, non-dimensional second and third moments of wing area.

using four sutures to a rod bent to follow the humerus and radius/ulna. It was only possible to use a single wing because a second right wing accurately matching the first was not available and the dorsal/ventral asymmetry of bird wings makes use of the left wing inappropriate. To balance the propeller, the stem of the rod attached to the wing was allowed to protrude through the propeller head. The wing was only slightly twisted (maximally 3°) but was strongly cambered, particularly at the base. At the 'elbow' joint between the humerus and ulna/radius, the wing depth (including camber and thickness) was 28.8% of the chord; at the 'wrist', over the alula base, this value was 24.1%; half-way between the alula and wing tip, it was 10%.

The wing, once attached to the rod, was scanned (Fig. 3B), and the appropriate moments were calculated. A print-out of the scanned image was used as a template for a wing model. The model wing was constructed from stiff, thin (0.3 mm) card glued to 1.4 mm diameter wire running half-way down the ventral surface of the wing. This resulted in a wing thickness at the position of mean chord of 4% of the chord. The single model wing was counterbalanced in the same way as the real wing. Again, the propeller head was considered when calculating wing moments (Table 2).

Angles of attack α were set by rotating the wire wing stems within the propeller head and measured using an inclinometer. The arbitrary 'representative' α was taken across the wing chord from the base of the alula to the tip of the innermost primary. The angle of incidence α′ was calculated as in Usherwood and Ellington (2002).

Frequency and Re

A variable power supply was used to drive the propeller head, using a 22 mm diameter, 12 V motor (RS) connected to a 24 mm diameter 7.2:1 gearhead. The rotational frequency was varied using the power supply until it reached 3.3 Hz for the model mayfly wing pairs, as judged with the use of a Drelloscop Strob 2009S07 stroboscope. Rotational frequency was set before and checked after each test. A rotational frequency of 3.3 Hz resulted in an *Re* based on the mean chord (Ellington, 1984f) of 1100, close to values estimated from video recordings of mayflies in ascending flight taken in the field and reasonable for the parameters described by Brodsky (1973) for the same species.

The rotational frequency for the quail wing and model was 12.5 Hz, resulting in an *Re* of 26 000 based on the mean chord. Askew et al. (2001) have observed a maximum downstroke angular flapping velocity ω of 190° s⁻¹ for a quail with a wing length of 95 mm. This corresponds to a maximum *Re* of 48 000, so 26 000 for the propeller implies that it is operating in a similar flow regime to the flapping

wing for most of the downstroke. The upstroke has little aerodynamic effect.

The mini-spinner for low Re: model mayfly wings
Vertical forces

The mini-spinner as shown in Fig. 2A has the motor, gearbox and propeller head oriented vertically. During steady revolution, a moment is created about the fulcrum due to the vertical force and the arm length to the right of the fulcrum. This is equal and opposite to the moment created by the tension force applied from a wire connected to the under-hook of a Mettler BasBal BB240 balance situated directly above, and the appropriate arm length to the left, of the fulcrum. This arrangement was calibrated with the repeated application of a 1 g mass to the centre of the propeller head, which resulted in an imperceptible deflection and produced values consistent with the geometry of the arrangement and the accuracy of the
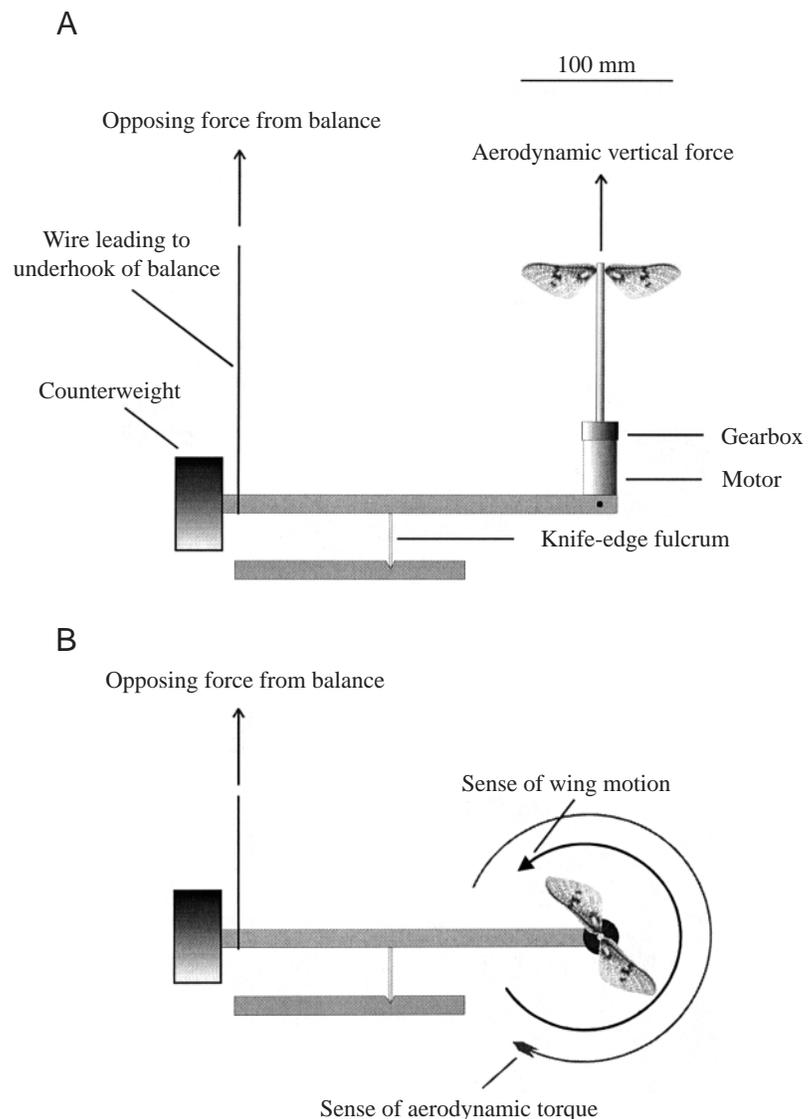

Fig. 2. The mini-spinner set up for small vertical force (A) and torque (B) measurements.

balance. The inherent linearity of the 'see-saw' arrangement was confirmed during set-up and testing. Thereafter, a single point calibration was sufficient. Five (or 10 at values of α of particular interest) vertical force measurements were made at each angle of attack.

Torques

Aerodynamic torques were measured by rotating the motor, gearbox and propeller head unit to a horizontal orientation as shown in Fig. 2B. During steady revolution, the moment about the fulcrum is equal to the aerodynamic torque from the revolving propeller head and wings. This torque can thus be calculated given the distance from the fulcrum to the wire attachment (140 mm) directly below the balance. The same number of measurements was made as for the vertical forces, and the aerodynamic effects of the motor head and stings were determined from tests without wings and removed.

Each vertical force and torque value was the mean of a pair of runs, starting with the wings in opposite positions. The measurements taken for each run consisted of a 'zero' and a 9 s average after steady revolution had been achieved. This takes into account any error due to an imbalance between the wings.

The mini-spinner for high Re*: real and model quail wings*

Vertical forces

Vertical forces were measured exactly as for the mayfly wings except that the moments were opposed by a stiff steel shim on which was glued a pair of strain gauges instead of the vertical wire leading to the balance: forces were too large and variable for the balance to provide accurate results. Signals from the strain gauges were amplified electronically before being sampled at 50 Hz using a Macintosh Quadra 650. Vertical force signals were averaged over 50 s. Five values from 10 paired runs, taking imbalance into account as above, were found for each angle of attack.

Torques

The forces due to the faster, heavier quail wings were such that the above method of measuring aerodynamic torques was impossible without adding large masses to stabilise the beam, which resulted in excessive loading on the strain-gauge shim. The torques were high enough, however, to be determined with sufficient accuracy from the power consumption of the motor. The current I passing through, and the voltage V across, the motor were measured five times for each angle of attack. The electrical power input (IV) is converted into aerodynamic power by the motor, with certain losses. These motor losses can be categorised (Electro-Craft Corporation, 1980) as being either speed-sensitive (which covers losses due to eddy currents, hysteresis, windage, friction, short circuits and brush contact) or torque-sensitive (winding resistance). The speed-sensitive components of electrical losses will be a constant C because a constant rotational frequency was used. C was determined by measuring the electrical power required to drive the motor with no wings
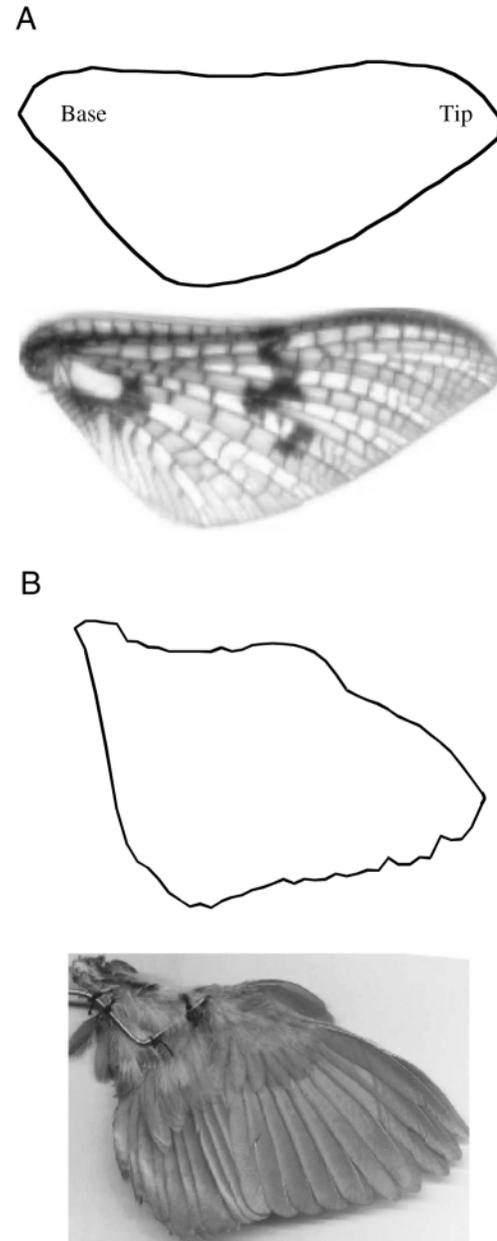

Fig. 3. Model and real wing planforms for mayfly (forewing) (A) and quail (B). Wing lengths R: real mayfly R=13 mm; model mayfly R=50 mm; model and real quail R=100.1 mm.

attached. The torque-sensitive power loss due to the winding $P_{winding}$ is given by:

$$P_{winding} = I^2 r_e, \tag{2}$$

where r_e is the resistance of the motor. Tests showed that r_e varied only very slightly with the time spent at the maximum torque, so the internal resistance of the motor did not change as a result of internal heating. Thus, the value of r_e taken for the stationary motor can also be used during revolution. Subtracting the two power losses from the power input yields the aerodynamic power P_{aero} required to overcome the aerodynamic torque on the wings:
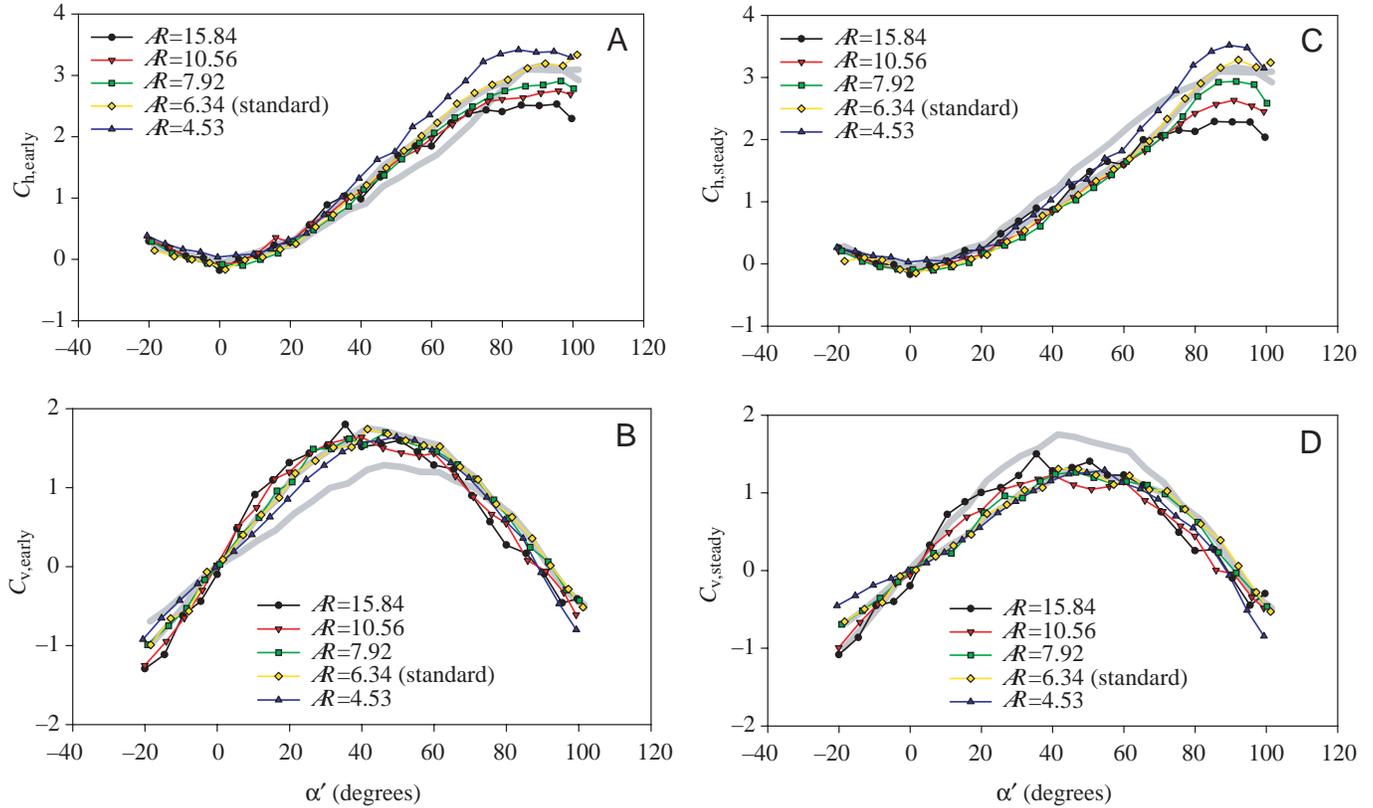
Fig. 4. Horizontal (C_h) (A,C) and vertical (C_v) (B,D) 'propeller' force coefficients over a range of angles of incidence α' under 'early' (A,B) and 'steady' (C,D) conditions for model hawkmoth wings with a range of aspect ratios (AR). Grey lines show 'early' and 'steady' coefficients for 'pooled' standard hawkmoth from Usherwood and Ellington (2002).

$$P_{aero} = (IV) - (I^2 r_e) - C, \qquad (3)$$

and torque Q is given by:

$$Q = P_{aero}/\Omega, \qquad (4)$$

where Ω is the angular velocity of propeller revolution.

Results

Aspect ratio series

Fig. 4 shows 'early' and 'steady' results for the hawkmoth wings over a range of aspect ratios. In each case, the 'pooled' data for the flat hawkmoth wings shown in Usherwood and Ellington (2002) are presented (both 'early' and 'steady' values) for comparison. The shift between 'early' and 'steady' values seen at intermediate angles of incidence for the standard hawkmoth wings is visible for all aspect ratios. The relationship between both $C_{h,early}$ and $C_{h,steady}$ (Fig. 4A,C) and α' at low angles is very consistent for wings of every AR tested. However, under both conditions, AR has a progressively greater effect at higher α'. Low-AR wings achieve considerably higher maximum horizontal force coefficients, peaking at $C_{h,early}=3.4$ and $C_{h,steady}=3.5$ near $\alpha'=90\,°$, while the highest-AR wings achieve maximum horizontal force coefficients of only 2.5 (Fig. 5).

The relationship between both $C_{v,early}$ and $C_{v,steady}$

(Fig. 4B,D) and α' is dependent on AR. While the maximum values reached, approximately 1.7 for $C_{v,early}$ and 1.3 for $C_{v,steady}$, are very similar for the entire range of aspect ratios and occur at similar values of α', between 40 and 60$\,°$, the initial gradients differ significantly. The relationships are
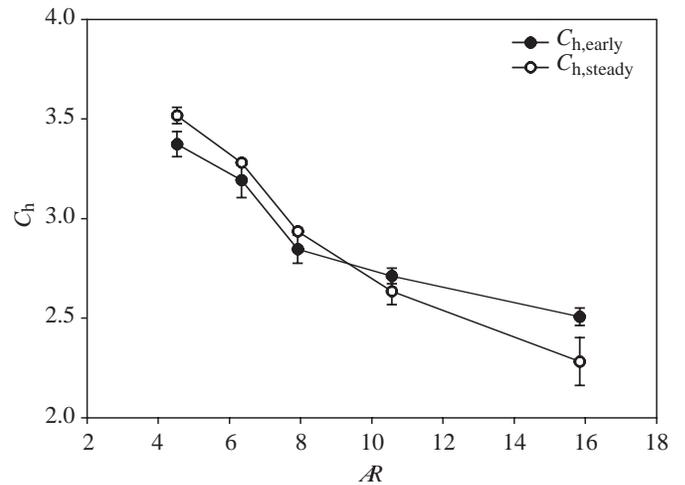

Fig. 5. The relationship between maximum horizontal force coefficient (C_h) (at an angle of attack α of 90$\,°$) and aspect ratio (AR) for revolving model hawkmoth wings under 'early' and 'steady' conditions. Error bars show ± 1 S.E.M. ($N=4$).

approximately linear between α'=–20 and +20°. The gradients $dC_v/d\alpha'$, with their 95% confidence intervals over this range, are given in Fig. 6. Lower-AR wings, and wings in 'steady' revolution, have lower gradients.

Bumblebee results

Fig. 7 shows the results for the *Bombus* wings. C_h and C_v, both 'early' and 'steady', show remarkably few differences compared with the 'pooled' hawkmoth results from Usherwood and Ellington (2002).

Steady results for range of species

Fig. 8 shows the 'steady' force coefficients for the model mayfly and model and real quail wings derived from force measurements using the 'mini-spinner'. These are plotted with the 'steady' coefficients for *Bombus* and pooled hawkmoth wings. Slight differences are visible in the horizontal force coefficients, with the mayfly showing lower coefficients (although with high standard errors) and the quail higher coefficients. The relationship between $C_{v,steady}$ and α' was remarkably consistent over the whole range of wings tested. All wings achieved maximum vertical force coefficients well above 1 at values of α' between 40 and 60°.

Deflections were visible in the revolving quail wings, with the tips of both real and model wings bending backwards, especially at higher values of α. The values of α' shown for the quail wings in Fig. 8 must therefore be considered approximate and lower than the true values.

Discussion

Steady high-lift mechanisms exist for a wide range of revolving wings

Force coefficients for a range of AR

Aspect ratio appears to have remarkably little effect on the force coefficients that can be achieved by revolving wings. Wings with values of AR from 4.53 to 15.84 produce indistinguishable maximum vertical force coefficients between α'=40° and 60° of 1.70 ('early') and 1.30 ('steady'). There is no distinct reduction in force coefficient that would be associated with 'stall', at least below α'=65° (and so of any relevance to insects hovering with a horizontal stroke plane), even for wings of very high AR. Above this angle, however, low-AR wings achieve higher force coefficients, which are dominated by C_h. At α=90°, there is a considerable range in C_h (Fig. 5): for AR=15.84, $C_{h,early}$=2.53 and $C_{h,steady}$=2.29; for AR=4.53, $C_{h,early}$=3.42 and $C_{h,steady}$=3.52. For the lower-AR wings, these values are well above those predicted for flat plates in steady translational flow. Ellington (1991) gives an approximate relationship for the drag coefficient of an infinite flat plate $C_{D,FP}$ appropriate for Re in the range 10^2 to 10^3:

$$C_{D,FP} = 1.95 + (50/Re),\qquad (5)$$

where $C_{D,FP}$ should be equivalent to $C_{h,steady}$ at α'=90°. Re is
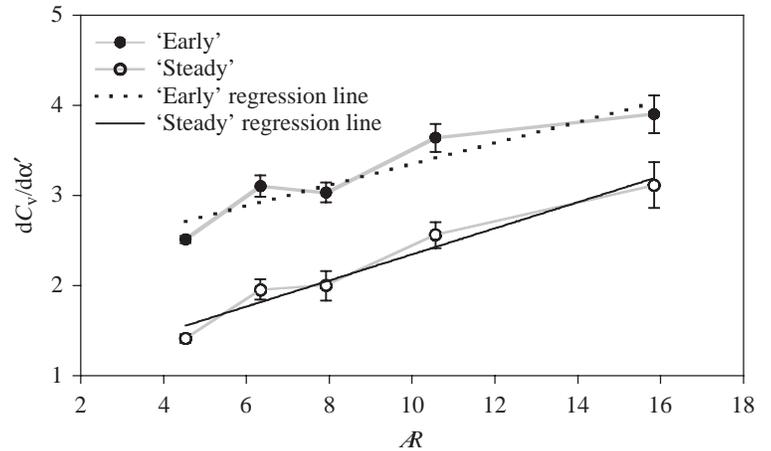

Fig. 6. The rate of change of vertical force coefficient (C_v) with angle of incidence (α'), $dC_v/d\alpha'$ for 'early' and 'steady' conditions from α'=–20 to +20° for model hawkmoth wings with a range of aspect ratios (AR). Bars show 95% confidence intervals (N=10). Differences both between high and low aspect ratios for either condition and between 'early' and 'steady' conditions for each aspect ratio are significant (P<0.01). The slopes of the regressions of $dC_v/d\alpha'$ against AR for 'early' and 'steady' conditions are not significantly different and average 0.130.
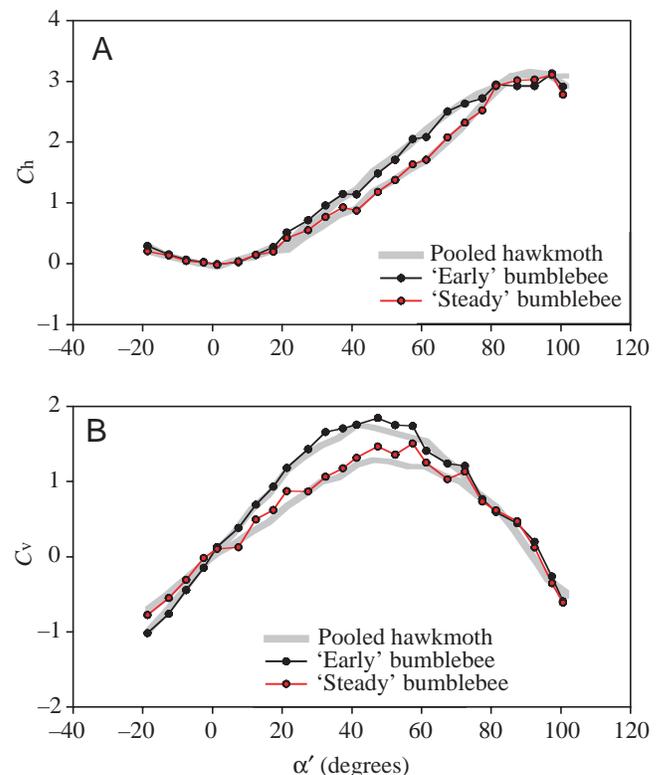

Fig. 7. Horizontal (C_h) (A) and vertical (C_v) (B) force coefficients under 'early' and 'steady' conditions for model bumblebee wings over a range of angles of incidence α'. Grey lines show 'early' (higher) and 'steady' (lower) coefficients for standard 'pooled' hawkmoth.
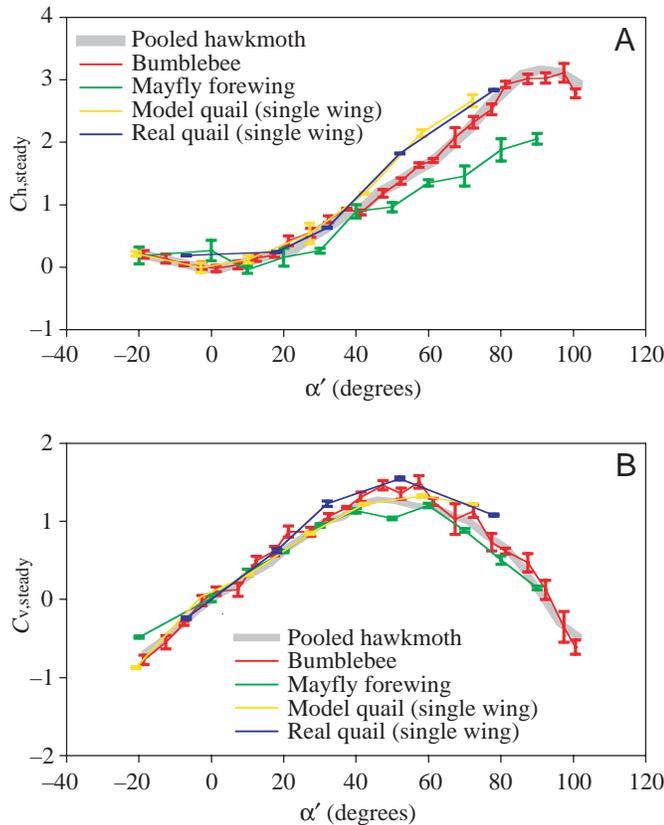
Fig. 8. Steady horizontal ($C_{h,steady}$) (A) and vertical ($C_{v,steady}$) (B) propeller coefficients for a range of wing types. Error bars show ±1 S.E.M. (N=4–10). α', angle of incidence.
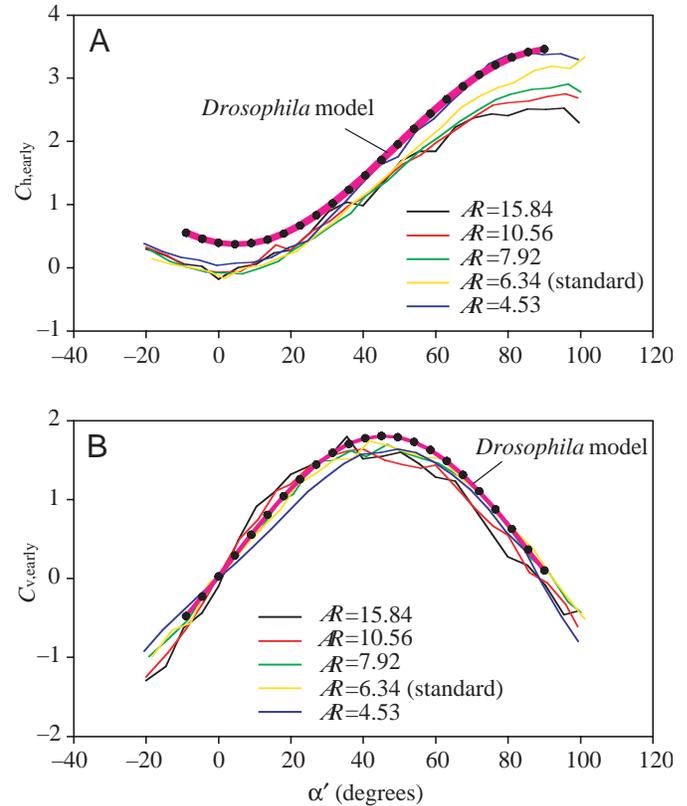

Fig. 9. 'Early' horizontal ($C_{h,early}$) (A) and vertical ($C_{v,early}$) (B) propeller coefficients for model hawkmoth wings over a range of aspect ratios (AR). The model relationship given by Dickinson et al. (1999) for *Drosophila* is overlaid. α', angle of incidence.

at least several thousand for the wings described here, so the predicted horizontal force coefficient is very close to 2 and varies only slightly over the range of Re covered by the wings. Furthermore, the three-dimensional effect of air 'sneaking' around the ends of the wing instead of flowing around its width would lead to even lower values of C_h (Hoerner, 1958) and incorrectly predict the direction of the relationship between maximum C_h and AR. The cause of the observed relationship is uncertain, but analogy with the vortices characteristically found over delta wings at high angles of incidence suggests that interference between leading- and trailing-edge vortices at high α' may be more significant for wings with higher AR.

These results suggest that blade-element analyses of revolving, perpendicular 'wings' may be in serious error if conventional, steady, two-dimensional force coefficients are used. In particular, older analyses of pectoral-fin swimming in fish (Blake, 1978) may have to be re-assessed.

Bumblebee force coefficients

The measurements made on the bumblebee wings are near the lower limits of the large propeller rig. However, all propeller coefficients ($C_{h,early}$, $C_{h,steady}$, $C_{v,early}$ and $C_{v,steady}$) agree so well with the values found for hawkmoth wings that little comment is possible, other than to observe that similar

aerodynamic mechanisms are almost certainly available to bumblebees and hawkmoths.

Steady force coefficients from mayfly to quail

Remarkably consistent, high force coefficients are achieved for simple, thin, flat model wings in steady revolution at Re from 1100 to 26 000; the real quail wing, with thickness and camber, not to mention feathers, produces very similar force coefficients. Drovetski (1996) gives polar diagrams from 0 to 25° for simple model galliform (game bird) wings. The video recordings of Askew et al. (2001) (and, consequently, the wing and wing model used in this study) do not show the trailing-edge notch described by Drovetski (1996); it appears that such a notch is present only in gliding flight or is an artefact of pinning the wings in a fully extended position. The maximum lift coefficients cited by Drovetski (1996) for wing models ranging from California quail *Callipepla californica* to turkey *Meleagris gallopavo* were between 0.61 and 0.80; it seems that some aspect of revolution may as much as double the vertical force coefficients. Values for blackbird *Turdus merula*, house sparrow *Passer domesticus* and mallard *Anas platyrhynchus* (Nachtigall and Kempf, 1971) range from 0.9 to 1.1, higher than for the galliforms of Drovetski (1996) but still considerably lower than those for revolving quail wings.
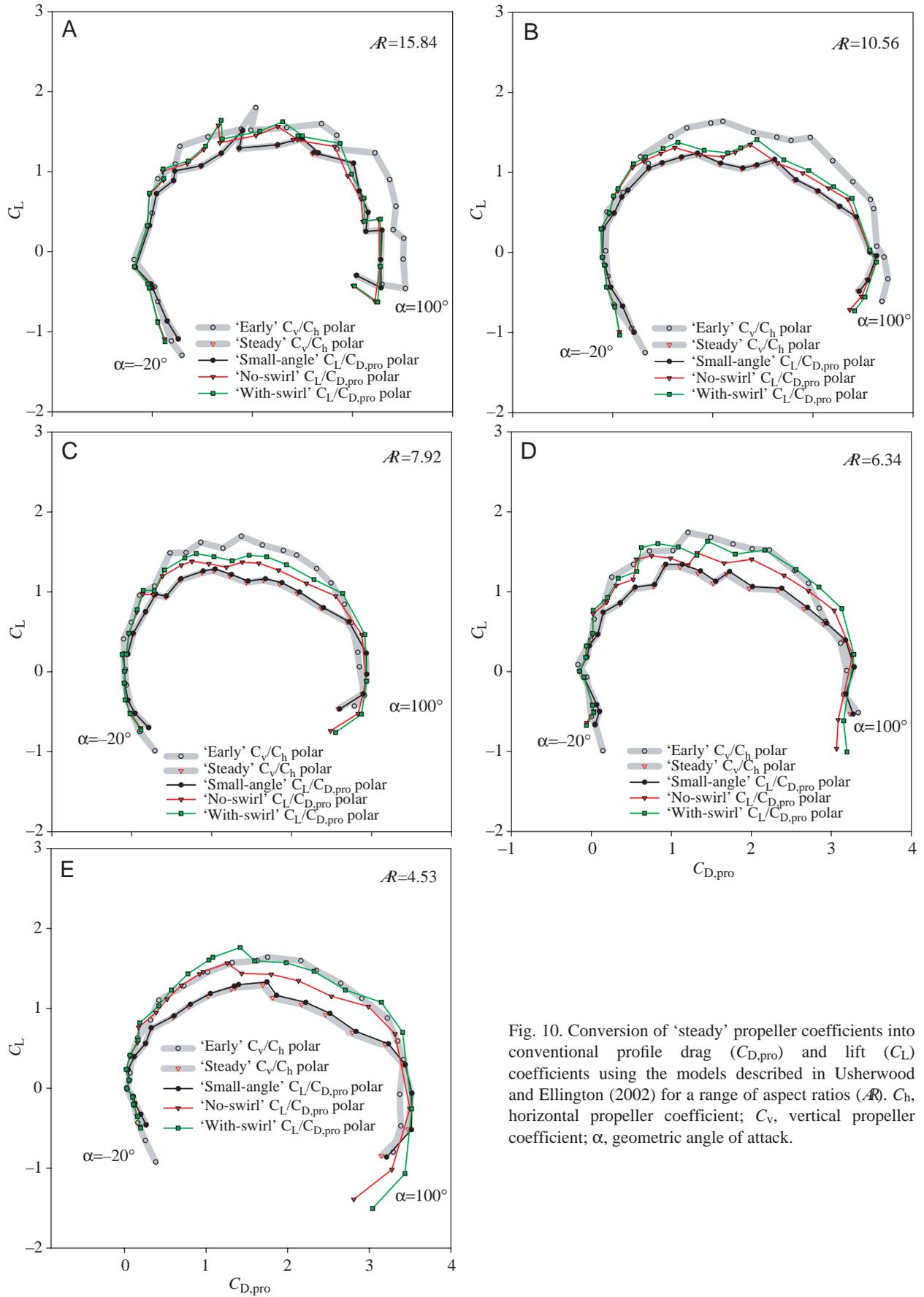
Fig. 10. Conversion of 'steady' propeller coefficients into conventional profile drag ($C_{D,pro}$) and lift (C_L) coefficients using the models described in Usherwood and Ellington (2002) for a range of aspect ratios ($A\!R$). C_h, horizontal propeller coefficient; C_v, vertical propeller coefficient; α, geometric angle of attack.
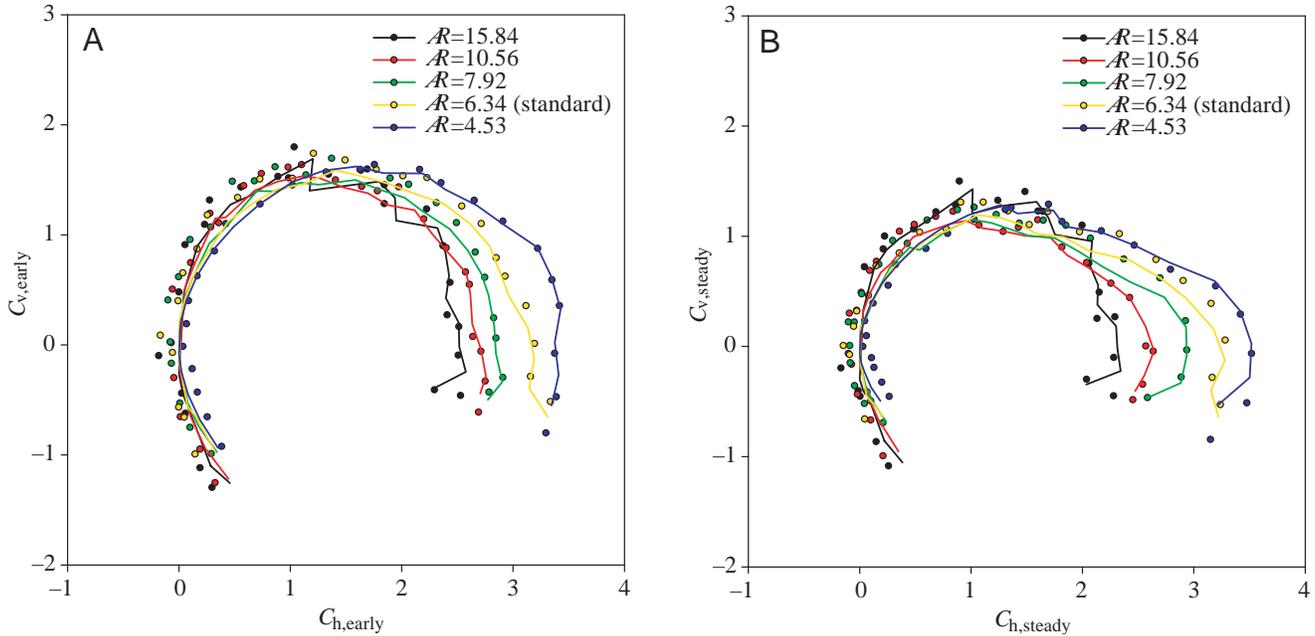
Fig. 11. Polar diagrams for model hawkmoth wings with a range of aspect ratios (AR) under 'early' (A) and 'steady' (B) conditions. Points give the measured values; lines are derived from the normal force relationship. C_h, horizontal force coefficient; C_v, vertical force coefficient.

High force coefficients as a robust phenomenon

The aerodynamic phenomenon resulting in high force coefficients, presumably associated with the creation and maintenance of leading-edge vortices, appears remarkably robust. Some of the force measurements on the flapping *Drosophila* model of Dickinson et al. (1999) are equivalent to the 'early' measurements described here, and their simple harmonic relationships are shown in Fig. 9 together with the 'early' results for the hawkmoth AR range. The *Drosophila* model shows a higher minimum horizontal force coefficient at low values of α because of relatively larger viscous forces. However, at higher values of α', there is very good agreement in both C_h and C_v with the values shown for hawkmoth planforms. If it is reasonable to suppose that shifts from 'early' to 'steady' conditions are relatively constant throughout the Re range, then it appears that similar force coefficients are possible from *Drosophila* ($Re \approx 200$) to quail ($Re \approx 26\,000$). If the mechanism for these high force coefficients is indeed the leading-edge vortex, then the insensitivity to Re is not as surprising as it may appear. Leading-edge vortices over sharp, thin delta wings are effective lift-producers for slow paper aeroplanes, Concorde and the space shuttle; a vast range of Re.

Further implications of aspect ratio
$dC_v/d\alpha'$ and aspect ratio

Fig. 6 shows relationships between aspect ratio and the rate of change of vertical force coefficient with angle of incidence, $dC_v/d\alpha'$. The relationships for both 'early' and 'steady' conditions are very similar: the gradients for regression lines through each plot on Fig. 6 are not significantly different. This phenomenon is well known for translating wings and is due

to the larger downwash of lower-AR wings, which produce greater forces for the same wing length. This results in a greater downwash angle ε, and so a smaller increase in 'effective angle of incidence' ($\alpha_r' = \alpha' - \varepsilon$) for a given increase in α'. The non-zero slope of the $dC_v/d\alpha'$ relationship for 'early' conditions shows that the 'early' induced downwash, while small, is not negligible; even before development of the propeller wake, the tip vortex appears to produce a downwash analogous to that for wings in translation. $C_{h,early}$ and $C_{v,early}$ therefore provide slight underestimates for $C_{D,pro}$ and C_L (see Usherwood and Ellington, 2002). However, the significance of this effect is minor compared with the surprisingly similar magnitudes of force coefficients for the AR range discussed above.

Implications of aspect ratio for wing design

The similarity in aerodynamic characteristics of wings over a considerable range of aspect ratio for $\alpha' < 65°$ suggests that, all other factors being equal, lower-AR wings should require less power to support body weight than higher-AR wings. For a given wing length R and wingbeat frequency n, the vertical force F_v during hovering is:

$$F_v \propto Sn^2, \tag{6}$$

and the aerodynamic power P_{aero} is:

$$P_{aero} \propto Sn^3 \tag{7}$$

because lift is related to area and the square of wing velocity, while power is proportional to wing area and the cube of wing velocity. The power required to support a given body weight is therefore proportional to n ($\propto P_{aero}/F_v$). The frequency and hence the power can be reduced by increasing wing area S

(equation 6) which, for a given wing length, is equivalent to decreasing the $A\!R$ (equation 1):

$$(P_{\text{aero}}/F_{\text{v}}) \propto n \propto \sqrt{A\!R}. \quad (8)$$

Clearly, many other aspects influence wing design in insects: aspect ratios may be determined by inertial power or weight considerations or by the energetics of unsteady or forward-flight aerodynamics. Also, manoeuvrability, visibility, protection when folded and developmental cost may all push wing design towards non-energetically adaptive optima. However, the above relationships do suggest a possible pressure towards broader wings in insects for which efficient hovering with a horizontal stroke plane is of selective significance.

The energetic advantage to butterflies of low-$A\!R$ wings is clearer. The large cabbage white *Pieris brassicae* hovers with a vertical stroke plane (Ellington 1984a), which means that horizontal force coefficients as defined here act in the vertical plane. While use is made of unsteady mechanisms such as the 'clap and fling', the benefits due to a low-$A\!R$ wing can be seen by considering steady propeller coefficients. The lowest-$A\!R$ wing tested had a maximum horizontal force coefficient of 3.52, 1.4 times that of the highest-$A\!R$ wing. Thus, lower-$A\!R$ wings produce larger forces because of their larger areas and because of their higher force coefficients. This should allow the butterfly to flap disproportionately slowly, lowering the power requirements for hovering.

Conversion of propeller coefficients into $C_{D,pro}$ and C_L

Fig. 10 shows the results for the $A\!R$ range of the three transformations described in Usherwood and Ellington (2002) that convert $C_{\text{h,steady}}$ and $C_{\text{v,steady}}$ into $C_{D,\text{pro}}$ and C_L, respectively. At values of α' greater than 50°, the models progressively underestimate C_L with increasing $A\!R$. However, both large-angle models give good fits to $C_{\text{h,early}}$ and $C_{\text{v,early}}$ for values of α' below 50°, which are more realistic for hovering insects.

The 'normal force relationship' is unaffected by induced downwash

The 'normal force relationship' between C_{h}, C_{v} and α described for standard hawkmoth wings in Usherwood and Ellington (2002) is also accurate at very low Re values (Dickinson et al., 1999) at high angles of attack. The effectiveness of the model for different $A\!R$, and its insensitivity to induced velocities, is shown in Fig. 11: the observed resultant force coefficient C_{R} can be accurately divided into C_{h} and C_{v} by:

$$C_{\text{h}} = C_{\text{R}}\sin\alpha \quad (9)$$
and
$$C_{\text{v}} = C_{\text{R}}\cos\alpha \quad (10)$$

respectively. The fits are very good, even at very high α', despite the various induced air velocities associated with the range of $A\!R$, and 'early' and 'steady' conditions.

In conclusion, the aerodynamics of revolving wings appears quite insensitive to variations in both wing morphology and kinematics: force coefficients for a range of model insect wings and for the wing of one small bird closely match those previously found for *Drosophila* wings. In addition, aspect ratio has remarkably little influence on aerodynamic force coefficients, at least at low-to-moderate angles of attack.

List of symbols

$A\!R$	aspect ratio
C	sum of speed-sensitive components of electrical power loss
$C_{D,\text{FP}}$	drag coefficient for a flat plate in perpendicular flow
$C_{D,\text{pro}}$	profile drag coefficient
C_{h}	horizontal force coefficient
C_L	lift coefficient
C_{R}	resultant force coefficient
C_{v}	vertical force coefficient
F_{v}	vertical force
I	electrical current
n	wingbeat frequency
P_{aero}	aerodynamic power
P_{winding}	power due to winding in electric motor
Q	torque
$\hat{r}_2(S)$	non-dimensional second moment of area
$\hat{r}_3(S)$	non-dimensional third moment of area
r_{e}	electrical resistance
R	wing length
Re	Reynolds number
S	area of a pair of wings
V	voltage
α	geometric angle of attack
α'	angle of incidence
α_{r}'	effective angle of incidence
ε	downwash angle
ω	downwash angular flapping velocity
Ω	angular velocity of the propeller

Subscripts

early	before propeller wake has developed (e.g. $C_{\text{v,early}}$)
steady	after propeller wake has developed (e.g. $C_{\text{v,steady}}$)

References

Askew, G. N., Marsh, R. L. and Ellington, C. P. (2001). The mechanical power output of the flight muscles of blue-breasted quail (*Coturnix chinensis*) during take-off. *J. Exp. Biol.* **204**, 3601–3619.
Blake, R. W. (1978). The mechanics of labriform locomotion. I. Labriform locomotion in the angelfish (*Pterophyllum eimekei*): an analysis of the power stroke. *J. Exp. Biol.* **82**, 255–271.
Brodsky, A. K. (1973). The swarming behaviour of mayflies (Ephemeroptera). *Entomol. Rev.* **52**, 33–39.
Casey, T. M. and Ellington, C. P. (1989). Energetics of insect flight. In *Energy Transformations in Cells and Organisms* (ed. W. Wieser and E. Gnaiger), pp. 200–210. Stuttgart: Georg Thieme Verlag.

Cooper, A. J. (1993). Limitations of bumblebee flight performance. PhD thesis, Cambridge University.

Dickinson, M. H., Lehmann, F.-O. and Sane, S. P. (1999). Wing rotation and the aerodynamic basis of insect flight. *Science* **284**, 1954–1960.

Drovetski, S. V. (1996). Influence of trailing-edge notch on flight performance of galliforms. *Auk* **113**, 802–810.

Dudley, R. (1995). Extraordinary flight performance of orchid bees (Apidae: Euglossini) hovering in heliox (80 % He/20 % O$_2$). *J. Exp. Biol.* **198**, 1065–1070.

Dudley, R. and Chai, P. (1996). Animal flight mechanics in physically variable gas mixtures. *J. Exp. Biol.* **199**, 1881–1885.

Dudley, R. and DeVries, P. J. (1990). Flight physiology of migrating *Urania fulgens* (Uraniidae) moths: kinematics and aerodynamics of natural free flight. *J. Comp. Physiol. A* **167**, 145–154.

Dudley, R. and Ellington, C. P. (1990a). Mechanics of forward flight in bumblebees. I. Kinematics and morphology. *J. Exp. Biol.* **148**, 19–52.

Dudley, R. and Ellington, C. P. (1990b). Mechanics of forward flight in bumblebees. II. Quasi-steady lift and power requirements. *J. Exp. Biol.* **148**, 53–88.

Electro-Craft Corporation (1980). *DC Motors Speed Controls Servo Systems*. Crewe: Electro-Craft.

Ellington, C. P. (1984a). The aerodynamics of hovering insect flight. I. The quasi-steady analysis. *Phil. Trans. R. Soc. Lond. B* **305**, 1–15.

Ellington, C. P. (1984b). The aerodynamics of hovering insect flight. II. Morphological parameters. *Phil. Trans. R. Soc. Lond. B* **305**, 17–40.

Ellington, C. P. (1984c). The aerodynamics of hovering insect flight. III. Kinematics. *Phil. Trans. R. Soc. Lond. B* **305**, 41–78.

Ellington, C. P. (1984d). The aerodynamics of hovering insect flight. IV. Aerodynamic mechanisms. *Phil. Trans. R. Soc. Lond. B* **305**, 79–113.

Ellington, C. P. (1984e). The aerodynamics of hovering insect flight. V. A vortex theory. *Phil. Trans. R. Soc. Lond. B* **305**, 115–144.

Ellington, C. P. (1984f). The aerodynamics of hovering insect flight. VI. Lift and power requirements. *Phil. Trans. R. Soc. Lond. B* **305**, 145–181.

Ellington, C. P. (1991). Aerodynamics and the origin of insect flight. *Adv. Insect Physiol.* **23**, 171–210.

Ellington, C. P., Van den Berg, C., Willmott, A. P. and Thomas, A. L. R. (1996). Leading-edge vortices in insect flight. *Nature* **384**, 626–630.

Graham, J. M. R. (1992). Wind tunnel measurements on a stalled horizontal axis wind turbine rotor. *IEEA Meeting, ECN Petten, NL*.

Hoerner, S. F. (1958). *Fluid-Dynamic Drag*. Bricktown, NJ: S. F. Hoerner.

Maxworthy, T. (1981). The fluid dynamics of insect flight. *Annu. Rev. Fluid Mech.* **13**, 329–350.

Nachtigall, W. and Kempf, B. (1971). Vergleichende Untersuchungen zur Flugbiologischen Funktion des Daumenfittichs (*Alula spuria*) bei Vögeln. *Z. Vergl. Physiol.* **71**, 326–341.

Norberg, U. M. (1975). Hovering flight of the pied flycatcher (*Ficedula hypoleuca*). In *Swimming and Flying in Nature*, vol. 2 (ed. T. Y. Wu, C. J. Brokaw and C. Brennen), pp. 869–881. New York: Plenum Press.

Norberg, U. M. (1976). Aerodynamics of hovering flight in the long-eared bat *Plecotus auritus*. *J. Exp. Biol.* **65**, 459–470.

Schlichting, H. (1968). *Boundary-Layer Theory*. New York: McGraw-Hill.

Sunada, S., Kawachi, K., Watanabe, I. and Azuma, A. (1993). Performance of a butterfly in take-off flight. *J. Exp. Biol.* **183**, 249–277.

Usherwood, J. R. and Ellington, C. P. (2002). The aerodynamics of revolving wings. I. Model hawkmoth wings. *J. Exp. Biol.* **205**, 1547–1564.

Vogel, S. (1981). *Life in Moving Fluids.* London: Willard Grant.

Weis-Fogh, T. (1973). Quick estimates of flight fitness in hovering animals, including novel mechanisms for lift production. *J. Exp. Biol.* **59**, 169–230.

Wells, D. J. (1993). Muscle performance in hovering hummingbirds. *J. Exp. Biol.* **178**, 39–57.